

# The LOCO-I Lossless Image Compression Algorithm: Principles and Standardization into JPEG-LS

Marcelo J. Weinberger, *Senior Member, IEEE*, Gadiel Seroussi, *Fellow, IEEE*, and Guillermo Sapiro, *Member, IEEE*

**Abstract**—LOCO-I (LOW COMPLEXITY LOSSLESS COMPRESSION for Images) is the algorithm at the core of the new ISO/ITU standard for lossless and near-lossless compression of continuous-tone images, JPEG-LS. It is conceived as a “low complexity projection” of the universal context modeling paradigm, matching its modeling unit to a simple coding unit. By combining simplicity with the compression potential of context models, the algorithm “enjoys the best of both worlds.” It is based on a simple fixed context model, which approaches the capability of the more complex universal techniques for capturing high-order dependencies. The model is tuned for efficient performance in conjunction with an extended family of Golomb-type codes, which are adaptively chosen, and an embedded alphabet extension for coding of low-entropy image regions. LOCO-I attains compression ratios similar or superior to those obtained with state-of-the-art schemes based on arithmetic coding. Moreover, it is within a few percentage points of the best available compression ratios, at a much lower complexity level. We discuss the principles underlying the design of LOCO-I, and its standardization into JPEG-LS.

**Index Terms**—Context modeling, geometric distribution, Golomb codes, lossless image compression, near-lossless compression, standards.

## I. INTRODUCTION

LOCO-I (LOW COMPLEXITY LOSSLESS COMPRESSION for Images) is the algorithm at the core of the new ISO/ITU standard for lossless and near-lossless compression of continuous-tone images, JPEG-LS. The algorithm was introduced in an abridged format in [1]. The standard evolved after successive refinements [2]–[6], and a complete specification can be found in [7]. However, the latter reference is quite obscure, and it omits the theoretical background that explains the success of the algorithm. In this paper, we discuss the theoretical foundations of LOCO-I and present a full description of the main algorithmic components of JPEG-LS.

Lossless data compression schemes often consist of two distinct and independent components: *modeling* and *coding*. The modeling part can be formulated as an inductive inference problem, in which the data (e.g., an image) is observed sample by sample in some predefined order (e.g., raster-scan, which will be the assumed order for images in the sequel). At each time instant  $t$ , and after having scanned past data  $x^t = x_1 x_2 \dots x_t$ , one wishes to make inferences on the next

sample value  $x_{t+1}$  by assigning a conditional probability distribution  $P(\cdot | x^t)$  to it. Ideally, the code length contributed by  $x_{t+1}$  is  $-\log P(x_{t+1} | x^t)$  bits (hereafter, logarithms are taken to the base 2), which averages to the entropy of the probabilistic model. In a *sequential* formulation, the distribution  $P(\cdot | x^t)$  is learned from the past and is available to the decoder as it decodes the past string sequentially. Alternatively, in a *two-pass* scheme the conditional distribution can be learned from the whole image in a first pass and must be sent to the decoder as header information.<sup>1</sup>

The conceptual separation between the modeling and coding operations [9] was made possible by the invention of the *arithmetic codes* [10], which can realize any probability assignment  $P(\cdot | \cdot)$ , dictated by the model, to a preset precision. These two milestones in the development of lossless data compression allowed researchers to view the problem merely as one of probability assignment, concentrating on the design of imaginative models for specific applications (e.g., image compression) with the goal of improving on compression ratios. Optimization of the sequential probability assignment process for images, inspired on the ideas of *universal modeling*, is analyzed in [11], where a relatively high complexity scheme is presented as a way to demonstrate these ideas. Rather than pursuing this optimization, the main objective driving the design of LOCO-I is to systematically “project” the image modeling principles outlined in [11] and further developed in [12], into a low complexity plane, both from a modeling and coding perspective. A key challenge in this process is that the above separation between modeling and coding becomes less clean under the low complexity coding constraint. This is because the use of a generic arithmetic coder, which enables the most general models, is ruled out in many low complexity applications, especially for software implementations.

Image compression models customarily consisted of a fixed structure, for which parameter values were adaptively learned. The model in [11], instead, is adaptive not only in terms of the parameter values, but also in structure. While [11] represented the best published compression results at the time (at the cost of high complexity), it could be argued that the improvement over the fixed model structure paradigm, best represented by the Sunset family of algorithms [13]–[16], was scant. The research leading to the CALIC algorithm [17], conducted in parallel to the development of LOCO-I, seems to confirm a pattern of diminishing returns. CALIC avoids some of the optimizations performed in [11], but by tuning the model more carefully to the image compression application, some compression gains are obtained. Yet, the improvement is not dramatic, even for the most

Manuscript received November 24, 1998; revised March 1, 2000. The associate editor coordinating the review of this manuscript and approving it for publication was Dr. Lina J. Karam.

M. J. Weinberger and G. Seroussi are with the Hewlett-Packard Laboratories, Palo Alto, CA 94304 USA (e-mail: marcelo@hpl.hp.com).

G. Sapiro was with Hewlett-Packard Laboratories, Palo Alto, CA 94304 USA. He is now with the Department of Electrical and Computer Engineering, University of Minnesota, Minneapolis, MN 55455 USA.

Publisher Item Identifier S 1057-7149(00)06129-7.

<sup>1</sup>A two-pass version of LOCO-I was presented in [8].

complex version of the algorithm [18]. More recently, the same observation applies to the TMW algorithm [19], which adopts a multiple-pass modeling approach. Actually, in many applications, a drastic complexity reduction can have more practical impact than a modest increase in compression. This observation suggested that judicious modeling, which seemed to be reaching a point of diminishing returns in terms of compression ratios, should rather be applied to obtain competitive compression at significantly lower complexity levels.

On the other hand, simplicity-driven schemes (e.g., the most popular version of the lossless JPEG standard [20]) propose minor variations of traditional DPCM techniques [21], which include Huffman coding [22] of prediction residuals obtained with some fixed predictor. These simpler techniques are fundamentally limited in their compression performance by the first order entropy of the prediction residuals, which in general cannot achieve total decorrelation of the data [23]. The compression gap between these simple schemes and the more complex ones is significant, although the FELICS algorithm [24] can be considered a first step in bridging this gap, as it incorporates adaptivity in a low complexity framework.

While maintaining the complexity level of FELICS, LOCO-I attains significantly better compression ratios, similar or superior to those obtained with state-of-the-art schemes based on arithmetic coding, but at a fraction of the complexity. In fact, as shown in Section VI, when tested over a benchmark set of images of a wide variety of types, LOCO-I performed within a few percentage points of the best available compression ratios (given, in practice, by CALIC), at a much lower complexity level. Here, complexity was estimated by measuring running times of software implementations made widely available by the authors of the respective algorithms.

In the sequel, our discussions will generally be confined to gray-scale images. For multicomponent (color) images, the JPEG-LS syntax supports both interleaved and noninterleaved (i.e., component by component) modes. In interleaved modes, possible correlation between color planes is used in a limited way, as described in the Appendix. For some color spaces (e.g., an RGB representation), good decorrelation can be obtained through simple lossless color transforms as a pre-processing step to JPEG-LS. Similar performance is attained by more elaborate schemes which do not assume prior knowledge of the color space (see, e.g., [25] and [26]).

JPEG-LS offers a lossy mode of operation, termed “near-lossless,” in which every sample value in a reconstructed image component is guaranteed to differ from the corresponding value in the original image by up to a preset (small) amount,  $\delta$ . In fact, in the specification [7], the lossless mode is just a special case of near-lossless compression, with  $\delta = 0$ . This paper will focus mainly on the lossless mode, with the near-lossless case presented as an extension in Section IV.

The remainder of this paper is organized as follows. Section II reviews the principles that guide the choice of model in lossless image compression, and introduces the basic components of LOCO-I as low complexity projections of these guiding principles. Section III presents a detailed description of the basic algorithm behind JPEG-LS culminating with a summary of all the steps of the algorithm. Section IV discusses the near-loss-

less mode, while Section V discusses variations to the basic configuration, including one based on arithmetic coding, which has been adopted for a prospective extension of the baseline JPEG-LS standard. In Section VI, compression results are reported for standard image sets. Finally, an Appendix lists various additional features in the standard, including the treatment of color images.

While modeling principles will generally be discussed in reference to LOCO-I as the algorithm behind JPEG-LS, specific descriptions will generally refer to LOCO-I/JPEG-LS, unless applicable to only one of the schemes.

## II. MODELING PRINCIPLES AND LOCO-I

### A. Model Cost and Prior Knowledge

In this section, we review the principles that guide the choice of model and, consequently, the resulting probability assignment scheme. In state-of-the-art lossless image compression schemes, this probability assignment is generally broken into the following components.

- 1) A prediction step, in which a value  $\hat{x}_{t+1}$  is guessed for the next sample  $x_{t+1}$  based on a finite subset (a *causal template*) of the available past data  $x^t$ .
- 2) The determination of a *context* in which  $x_{t+1}$  occurs. The context is, again, a function of a (possibly different) causal template.
- 3) A probabilistic model for the *prediction residual* (or error signal)  $\epsilon_{t+1} \triangleq x_{t+1} - \hat{x}_{t+1}$ , conditioned on the context of  $x_{t+1}$ .

This structure was pioneered by the Sunset algorithm [13].

*Model Cost:* A probability assignment scheme for data compression aims at producing a code length which approaches the empirical entropy of the data. Lower entropies can be achieved through higher order conditioning (larger contexts). However, this implies a larger number  $K$  of parameters in the statistical model, with an associated *model cost* [27] which could offset the entropy savings. This cost can be interpreted as capturing the penalties of “context dilution” occurring when count statistics must be spread over too many contexts, thus affecting the accuracy of the corresponding estimates. The per-sample asymptotic model cost is given by  $(K \log n)/(2n)$ , where  $n$  is the number of data samples [28]. Thus, the number of parameters plays a fundamental role in modeling problems, governing the above “tension” between entropy savings and model cost [27]. This observation suggests that the choice of model should be guided by the use, whenever possible, of available *prior knowledge* on the data to be modeled, thus avoiding unnecessary “learning” costs (i.e., overfitting). In a context model,  $K$  is determined by the number of free parameters defining the coding distribution at each context and by the number of contexts.

*Prediction:* In general, the predictor consists of a fixed and an adaptive component. When the predictor is followed by a zero-order coder (i.e., no further context modeling is performed), its contribution stems from it being the only “decorrelation” tool. When used in conjunction with a context model, however, the contribution of the predictor is more subtle, espe-

cially for its adaptive component. In fact, prediction may seem redundant at first, since the same contextual information that is used to predict is also available for building the coding model, which will eventually learn the “predictable” patterns of the data and assign probabilities accordingly. The use of two different modeling tools based on the same contextual information is analyzed in [12], and the interaction is also explained in terms of model cost. The first observation, is that prediction turns out to reduce the number of coding parameters needed for modeling high order dependencies. This is due to the existence of multiple conditional distributions that are similarly shaped but centered at different values. By predicting a deterministic, context-dependent value  $\hat{x}_{t+1}$  for  $x_{t+1}$ , and considering the (context)-conditional probability distribution of the prediction residual  $\epsilon_{t+1}$  rather than that of  $x_{t+1}$  itself, we allow for similar probability distributions on  $\epsilon$ , which may now be all centered at zero, to merge in situations when the original distributions on  $x$  would not. Now, while the fixed component of the predictor can easily be explained as reflecting our prior knowledge of typical structures in the data, leading, again, to model cost savings, the main contribution in [12] is to analyze the adaptive component. Notice that adaptive prediction also learns patterns through a model (with a number  $K'$  of parameters), which has an associated learning cost. This cost should be weighted against the potential savings of  $O(K(\log n)/n)$  in the coding model cost. A first indication that this trade-off might be favorable is given by the predictability bound in [29] (analogous to the coding bound in [28]), which shows that the per-sample model cost for prediction is  $O(K'/n)$ , which is asymptotically negligible with respect to the coding model cost. The results in [12] confirm this intuition and show that it is worth increasing  $K'$  while reducing  $K$ . As a result, [12] proposes the basic paradigm of using a large model for adaptive prediction which in turn allows for a smaller model for adaptive coding. This paradigm is also applied, for instance, in [17].

*Parametric Distributions:* Prior knowledge on the structure of images to be compressed can be further utilized by fitting parametric distributions with few parameters per context to the data. This approach allows for a larger number of contexts to capture higher order dependencies without penalty in overall model cost. Although there is room for creative combinations, the widely accepted observation [21] that prediction residuals in continuous-tone images are well modeled by a *two-sided geometric distribution* (TSGD) makes this model very appealing in image coding. It is used in [11] and requires only two parameters (representing the rate of decay and the shift from zero) per context, as discussed in Section III-B1.

The optimization of the above modeling steps, inspired on the ideas of universal modeling, is demonstrated in [11]. In this scheme, the context for  $x_{t+1}$  is determined out of differences  $x_{t_i} - x_{t_j}$ , where the pairs  $(t_i, t_j)$  correspond to adjacent locations within a fixed causal template, with  $t_i, t_j \leq t$ . Each difference is adaptively quantized based on the concept of stochastic complexity [27], to achieve an optimal number of contexts. The prediction step is accomplished with an adaptively optimized, context-dependent function of neighboring sample values (see [11, (Eq. 3.2)]). The prediction residuals, modeled by a TSGD, are arithmetic-encoded and the resulting code length is asymptotically optimal in a certain broad class of processes used to model the data [30].

totically optimal in a certain broad class of processes used to model the data [30].

## B. Application to LOCO-I

In this section, we introduce the basic components of LOCO-I as low complexity projections of the guiding principles presented in Section II-A. The components are described in detail in Section III.

*Predictor:* The predictor in LOCO-I is context-dependent, as in [11]. It also follows classical autoregressive (AR) models, including an affine term (see, e.g., [31]).<sup>2</sup> This affine term is adaptively optimized, while the dependence on the surrounding samples is through fixed coefficients. The fixed component of the predictor further incorporates prior knowledge by switching among three simple predictors, thus resulting in a nonlinear function with a rudimentary edge detecting capability. The adaptive term is also referred to as “bias cancellation,” due to an alternative interpretation (see Section III-A).

*Context Model:* A very simple context model, determined by quantized gradients as in [11], is aimed at approaching the capability of the more complex universal context modeling techniques for capturing high-order dependencies. The desired small number of free statistical parameters is achieved by adopting, here as well, a TSGD model, which yields two free parameters per context.

*Coder:* In a low complexity framework, the choice of a TSGD model is of paramount importance since it can be efficiently encoded with an extended family of Golomb-type codes [32], which are adaptively selected [33] (see also [34]). The on-line selection strategy turns out to be surprisingly simple, and it is derived by reduction of the family of optimal prefix codes for TSGDs [35]. As a result, adaptive symbol-by-symbol coding is possible at very low complexity, thus avoiding the use of the more complex arithmetic coders.<sup>3</sup> In order to address the redundancy of symbol-by-symbol coding in the low entropy range (“flat” regions), an alphabet extension is embedded in the model (“run” mode). In JPEG-LS, run lengths are adaptively coded using *block-MELCODE*, an adaptation technique for Golomb-type codes [2], [36].

*Summary:* The overall simplicity of LOCO-I/JPEG-LS can be mainly attributed to its success in matching the complexity of the modeling and coding units, combining simplicity with the compression potential of context models, thus “enjoying the best of both worlds.” The main blocks of the algorithm are depicted in Fig. 1, including the causal template actually employed. The shaded area in the image icon at the left of the figure represents the scanned past data  $x^t$ , on which prediction and context modeling are based, while the black dot represents the sample  $x_{t+1}$  currently encoded. The switches labeled *mode* select operation in “regular” or “run” mode, as determined from  $x^t$  by a simple region “flatness” criterion.

<sup>2</sup>A specific linear predicting function is demonstrated in [11], as an example of the general setting. However, all implementations of the algorithm also include an affine term, which is estimated through the average of past prediction errors, as suggested in [11, p. 583].

<sup>3</sup>The use of Golomb codes in conjunction with context modeling was pioneered in the FELICS algorithm [24].

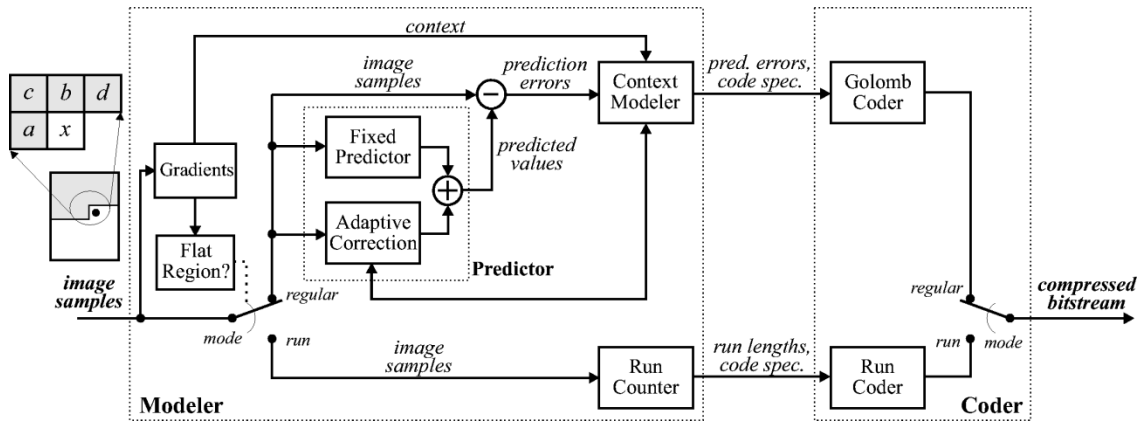


Fig. 1. JPEG-LS: Block diagram.

### III. DETAILED DESCRIPTION OF JPEG-LS

The prediction and modeling units in JPEG-LS are based on the causal template depicted in Fig. 1, where  $x$  denotes the current sample, and  $a, b, c$ , and  $d$ , are neighboring samples in the relative positions shown in the figure.<sup>4</sup> The dependence of  $a, b, c, d$ , and  $x$ , on the time index  $t$  has been deleted from the notation for simplicity. Moreover, by abuse of notation, we will use  $a, b, c, d$ , and  $x$  to denote both the *values* of the samples and their *locations*. By using the template of Fig. 1, JPEG-LS limits its image buffering requirement to one scan line.

#### A. Prediction

Ideally, the value guessed for the current sample  $x$  should depend on  $a, b, c$ , and  $d$  through an adaptive model of the local edge direction. While our complexity constraints rule out this possibility, some form of edge detection is still desirable. In LOCO-I/JPEG-LS, a fixed predictor performs a primitive test to detect vertical or horizontal edges, while the adaptive part is limited to an *integer* additive term, which is context-dependent as in [11] and reflects the affine term in classical AR models (e.g., [31]). Specifically, the fixed predictor in LOCO-I/JPEG-LS guesses

$$\hat{x}_{\text{MED}} \triangleq \begin{cases} \min(a, b), & \text{if } c \geq \max(a, b) \\ \max(a, b), & \text{if } c \leq \min(a, b) \\ a + b - c, & \text{otherwise.} \end{cases} \quad (1)$$

The predictor (1) switches between three simple predictors: it tends to pick  $b$  in cases where a vertical edge exists left of the current location,  $a$  in cases of an horizontal edge above the current location, or  $a + b - c$  if no edge is detected. The latter choice would be the value of  $x$  if the current sample belonged to the “plane” defined by the three neighboring samples with “heights”  $a, b$ , and  $c$ . This expresses the expected smoothness of the image in the absence of edges. The predictor (1) has been used in image compression applications [37], under a different interpretation: The guessed value is seen as the *median* of three

fixed predictors,  $a, b$ , and  $a + b - c$ . Combining both interpretations, this predictor was renamed during the standardization process “median edge detector” (MED).

As for the integer adaptive term, it effects a context-dependent translation. Therefore, it can be interpreted as part of the estimation procedure for the TSGD. This procedure is discussed in Section III-B. Notice that  $d$  is employed in the adaptive part of the predictor, but not in (1).

#### B. Context Modeling

As noted in Section II-A, reducing the number of parameters is a key objective in a context modeling scheme. This number is determined by the number of free parameters defining the coding distribution at each context and by the number of contexts.

##### 1) Parameterization:

*TSGD Model:* It is a widely accepted observation [21] that the global statistics of residuals from a fixed predictor in continuous-tone images are well-modeled by a TSGD centered at zero. According to this distribution, the probability of an integer value  $\epsilon$  of the prediction error is proportional to  $\theta^{|\epsilon|}$ , where  $\theta \in (0, 1)$  controls the two-sided exponential decay rate. However, it was observed in [15] that a dc offset is typically present in *context-conditioned* prediction error signals. This offset is due to integer-value constraints and possible bias in the prediction step. Thus, a more general model, which includes an additional *offset parameter*  $\mu$ , is appropriate. Letting  $\mu$  take noninteger values, the two adjacent modes often observed in empirical context-dependent histograms of prediction errors are also better captured by this model. We break the fixed prediction offset into an integer part  $R$  (or “bias”), and a fractional part  $s$  (or “shift”), such that  $\mu = R - s$ , where  $0 \leq s < 1$ . Thus, the TSGD parametric class  $P_{(\theta, \mu)}$ , assumed by LOCO-I/JPEG-LS for the residuals of the fixed predictor at each context, is given by

$$P_{(\theta, \mu)}(\epsilon) = C(\theta, s)\theta^{|\epsilon - R + s|}, \quad \epsilon = 0, \pm 1, \pm 2, \dots \quad (2)$$

where  $C(\theta, s) = (1 - \theta)/(\theta^{1-s} + \theta^s)$  is a normalization factor. The bias  $R$  calls for an integer adaptive term in the predictor. In the sequel, we assume that this term is tuned to cancel  $R$ , producing average residuals between distribution modes located

<sup>4</sup>The causal template in [1] includes an additional sample,  $e$ , West of  $a$ . This location was discarded in the course of the standardization process as its contribution was not deemed to justify the additional context storage required [4].

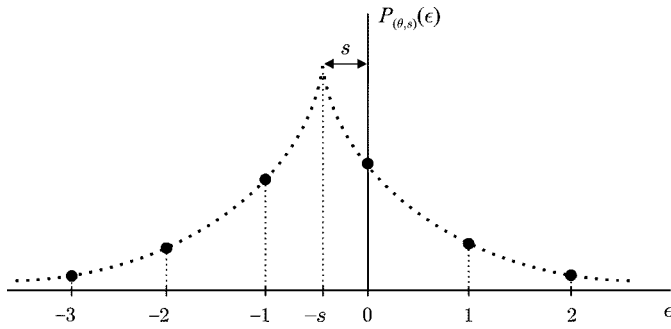


Fig. 2. Two-sided geometric distribution.

at 0 and  $-1$  (see Section III-B3). Consequently, after adaptive prediction, the model of (2) reduces in LOCO-I/JPEG-LS to

$$P_{(\theta,s)}(\epsilon) = C(\theta, s)\theta^{|\epsilon+s|}, \quad \epsilon = 0, \pm 1, \pm 2, \dots \quad (3)$$

where  $0 < \theta < 1$  and  $0 \leq s < 1$ , as above. This reduced range for the offset is matched to the codes presented in Section III-C, but any unit interval could be used in principle (the preference of  $-1$  over  $+1$  is arbitrary). The model of (3) is depicted in Fig. 2. The TSGD centered at zero corresponds to  $s = 0$ , and, when  $s = 1/2$ ,  $P_{(\theta,s)}$  is a bi-modal distribution with equal peaks at  $-1$  and  $0$ . Notice that the parameters of the distribution are context-dependent, even though this fact is omitted by our notation. Two-sided geometric distributions are extensively studied in [33]–[35]. Their low complexity adaptive coding is further investigated in [38]. The application of these low complexity techniques to LOCO-I/JPEG-LS is studied in Section III-C.

*Error Residual Alphabet in JPEG-LS:* The image alphabet, assumed infinite in (3), has a finite size  $\alpha$  in practice. For a given prediction  $\hat{x}$ ,  $\epsilon$  takes on values in the range  $-\hat{x} \leq \epsilon < \alpha - \hat{x}$ . Since  $\hat{x}$  is known to the decoder, the actual value of the prediction residual can be reduced, modulo  $\alpha$ , to a value between  $-\lceil \alpha/2 \rceil$  and  $\lceil \alpha/2 \rceil - 1$ . This is done in LOCO-I/JPEG-LS, thus remapping large prediction residuals to small ones. Merging the “tails” of peaked distributions with their central part does not significantly affect the two-sided geometric behavior. While this observation holds for smooth images, this remapping is especially suited also for, e.g., compound documents, as it assigns a large probability to sharp transitions. In the common case  $\alpha = 2^\beta$ , it consists of just interpreting the  $\beta$  least significant bits of  $\epsilon$  in 2’s complement representation.<sup>5</sup> Since  $\alpha$  is typically quite large, we will continue to use the infinite alphabet model (3), although the *reduced* prediction residuals, still denoted by  $\epsilon$ , belong to the finite range  $-\lceil \alpha/2 \rceil, \lceil \alpha/2 \rceil - 1$ .

## 2) Context Determination:

*General Approach:* The context that conditions the encoding of the current prediction residual in JPEG-LS is built out of the differences  $g_1 = d - b$ ,  $g_2 = b - c$ , and  $g_3 = c - a$ . These differences represent the local gradient, thus capturing the level of activity (smoothness, edginess) surrounding a sample, which governs the statistical behavior of prediction errors. Notice that this approach differs from the one adopted in the Sunset family [16] and other schemes, where the context is built out of

<sup>5</sup>A higher complexity remapping is discussed in [39].

the prediction errors incurred in previous encodings. By symmetry,<sup>6</sup>  $g_1, g_2$ , and  $g_3$  influence the model in the same way. Since further model size reduction is obviously needed, each difference  $g_j, j = 1, 2, 3$ , is quantized into a small number of approximately *equiprobable*, connected regions by a quantizer  $\kappa(\cdot)$  independent of  $j$ . This quantization aims at maximizing the *mutual information* between the current sample value and its context, an information-theoretic measure of the amount of information provided by the conditioning context on the sample value to be modeled. We refer to [11] and [12] for an in-depth theoretical discussion of these issues.

In principle, the number of regions into which each context difference is quantized should be adaptively optimized. However, the low complexity requirement dictates a fixed number of “equiprobable” regions. To preserve symmetry, the regions are indexed  $-T, \dots, -1, 0, 1, \dots, T$ , with  $\kappa(g) = -\kappa(-g)$ , for a total of  $(2T + 1)^3$  different contexts. A further reduction in the number of contexts is obtained after observing that, by symmetry, it is reasonable to assume that

$$\begin{aligned} \text{Prob}\{\epsilon_{t+1} = \Delta \mid C_t = [q_1, q_2, q_3]\} \\ = \text{Prob}\{\epsilon_{t+1} = -\Delta \mid C_t = [-q_1, -q_2, -q_3]\} \end{aligned}$$

where  $C_t$  represents the quantized context triplet and  $q_j = \kappa(g_j), j = 1, 2, 3$ . Hence, if the first nonzero element of  $C_t$  is negative, the encoded value is  $-\epsilon_{t+1}$ , using context  $-C_t$ . This is anticipated by the decoder, which flips the error sign if necessary to obtain the original error value. By merging contexts of “opposite signs,” the total number of contexts becomes  $((2T + 1)^3 + 1)/2$ .

*Contexts in JPEG-LS:* For JPEG-LS,  $T = 4$  was selected, resulting in 365 contexts. This number balances storage requirements (which are roughly proportional to the number of contexts) with high-order conditioning. In fact, due to the parametric model of (3), more contexts could be afforded for medium-sized to large images, without incurring an excessive model cost. However, the compression improvement is marginal and does not justify the increase in resources [4]. For small images, it is possible to reduce the number of contexts within the framework of the standard, as discussed below.

To complete the definition of the contexts in JPEG-LS, it remains to specify the boundaries between quantization regions. For an 8-bit/sample alphabet, the default quantization regions are  $\{0\}, \pm\{1, 2\}, \pm\{3, 4, 5, 6\}, \pm\{7, 8, \dots, 20\}, \pm\{e \mid e \geq 21\}$ . However, the boundaries are adjustable parameters, except that the central region must be  $\{0\}$ . In particular, a suitable choice collapses quantization regions, resulting in a smaller effective number of contexts, with applications to the compression of small images. For example, a model with 63 contexts ( $T = 2$ ), was found to work best for the  $64 \times 64$ -tile size used in the FlashPix™ file format [40]. Through appropriate scaling, default boundary values are also provided for general alphabet sizes  $\alpha$  [3], [7].

*3) Adaptive Correction:* As mentioned in Sections III-A and III-B1, the adaptive part of the predictor is context-based and it

<sup>6</sup>Here, we assume that the class of images to be encoded is essentially symmetric with respect to horizontal/vertical, left/right, and top/bottom transpositions, as well as the sample value “negation” transformation  $x \rightarrow (\alpha - 1 - x)$ .

is used to “cancel” the integer part  $R$  of the offset due to the fixed predictor. As a result, the context-dependent shift in the distributions (3) was restricted to the range  $0 \leq s < 1$ . This section discusses how this adaptive correction (or *bias cancellation*) is performed at low complexity.

*Bias Estimation:* In principle, *maximum-likelihood* (ML) estimation of  $R$  in (2) would dictate a bias cancellation procedure based on the *median* of the prediction errors incurred so far in the context by the fixed predictor (1). However, storage constraints rule out this possibility. Instead, an estimate based on the *average* could be obtained by just keeping a count  $N$  of context occurrences, and a cumulative sum  $D$  of fixed prediction errors incurred so far in the context. Then, a *correction value*  $C'$  could be computed as the rounded average

$$C' = \lceil D/N \rceil \quad (4)$$

and added to the fixed prediction  $\hat{x}_{\text{MED}}$ , to offset the prediction bias. This approach, however, has two main problems. First, it requires a general division, in opposition to the low complexity requirements of LOCO-I/JPEG-LS. Second, it is very sensitive to the influence of “outliers,” i.e., atypical large errors can affect future values of  $C'$  until it returns to its typical value, which is quite stable.

To solve these problems, first notice that (4) is equivalent to

$$D = N \cdot C' + B'$$

where the integer  $B'$  satisfies  $-N < B' \leq 0$ . It is readily verified, by setting up a simple recursion, that the correction value can be implemented by storing  $B'$  and  $C'$ , and adjusting both for each occurrence of the context. The *corrected* prediction error  $\epsilon$  is first added to  $B'$ , and then  $N$  is subtracted or added until the result is in the desired range  $(-N, 0]$ . The number of subtractions/additions of  $N$  prescribes the adjustment for  $C'$ .

*Bias Computation in JPEG-LS:* The above procedure is further modified in LOCO-I/JPEG-LS by limiting the number of subtractions/additions to one per update, and then “forcing” the value of  $B'$  into the desired range, if needed. Specifically,  $C'$  and  $B'$  are replaced by approximate values  $C$  and  $B$ , respectively, which are initialized to zero and updated according to the division-free procedure shown in Fig. 3 (in C-language style). The procedure increments (resp. decrements) the correction value  $C$  each time  $B > 0$  (resp.  $B \leq -N$ ). At this time,  $B$  is also adjusted to reflect the change in  $C$ . If the increment (resp. decrement) is not enough to bring  $B$  to the desired range (i.e., the adjustment in  $C$  was limited),  $B$  is clamped to 0 (resp.  $-N + 1$ ). This procedure will tend to produce average prediction residuals in the interval  $(-1, 0]$ , with  $C$  serving as an estimate (albeit not the ML one) of  $R$ . Notice that  $-B/N$  is an estimate of the residual fractional shift parameter  $s$  (again, not the ML one). To reduce storage requirements,  $C$  is not incremented (resp. decremented) over 127 (resp. under  $-128$ ). Mechanisms for “centering” image prediction error distributions, based on integer offset models, are described in [15] and [17].

### C. Coding

To encode corrected prediction residuals distributed according to the TSGD of (3), LOCO-I/JPEG-LS uses a minimal

```

B = B + ε; /* accumulate prediction residual */
N = N + 1; /* update occurrence counter */
/* update correction value and shift statistics */
if ( B ≤ -N ) {
    C = C - 1; B = B + N;
    if ( B ≤ -N ) B = -N + 1;
}
else if ( B > 0 ) {
    C = C + 1; B = B - N;
    if ( B > 0 ) B = 0;
}

```

Fig. 3. Bias computation procedure.

complexity subfamily of the family of optimal prefix codes for TSGDs, recently characterized in [35]. The coding unit also implements a low complexity adaptive strategy to *sequentially* select a code among the above sub-family. In this subsection, we discuss the codes of [35] and the principles guiding general adaptation strategies, and show how the codes and the principles are simplified to yield the adopted solution.

1) *Golomb Codes and Optimal Prefix Codes for the TSGD:* The optimal codes of [35] are based on *Golomb codes* [32], whose structure enables simple calculation of the code word of any given sample, without recourse to the storage of code tables, as would be the case with unstructured, generic Huffman codes. In an adaptive mode, a structured family of codes further relaxes the need of dynamically updating code tables due to possible variations in the estimated parameters (see, e.g., [41]).

Golomb codes were first described in [32], as a means for encoding run lengths. Given a positive integer parameter  $m$ , the  $m$ th order Golomb code  $G_m$  encodes an integer  $y \geq 0$  in two parts: a *unary* representation of  $\lfloor y/m \rfloor$ , and a *modified binary* representation of  $y \bmod m$  (using  $\lfloor \log m \rfloor$  bits if  $y < 2^{\lfloor \log m \rfloor} - m$  and  $\lfloor \log m \rfloor$  bits otherwise). Golomb codes are optimal [42] for *one-sided geometric distributions* (OSGDs) of the nonnegative integers, i.e., distributions of the form  $(1-\theta)\theta^y$ , where  $0 < \theta < 1$ . Thus, for every  $\theta$  there exists a value of  $m$  such that  $G_m$  yields the shortest average code length over all uniquely decipherable codes for the nonnegative integers.

The special case of Golomb codes with  $m = 2^k$  leads to very simple encoding/decoding procedures: the code for  $y$  is constructed by appending the  $k$  least significant bits of  $y$  to the unary representation of the number formed by the remaining higher order bits of  $y$  (the simplicity of the case  $m = 2^k$  was already noted in [32]). The length of the encoding is  $k + 1 + \lfloor y/2^k \rfloor$ . We refer to codes  $G_{2^k}$  as *Golomb-power-of-2* (GPO2) codes.

In the characterization of optimal prefix codes for TSGDs in [35], the parameter space  $(\theta, s)$  is partitioned into regions, and a different optimal prefix code corresponds to each region ( $s \leq 1/2$  is assumed, since the case  $s > 1/2$  can be reduced to the former by means of the reflection/shift transformation  $\epsilon \rightarrow -(\epsilon + 1)$  on the TSG-distributed variable  $\epsilon$ ). Each region is associated with an  $m$ th order Golomb code, where the parameter  $m$  is a function of the values of  $\theta$  and  $s$  in the region. Depending on the region, an optimal code from [35] encodes an integer  $\epsilon$  either by applying a region-dependent modification of  $G_m$  to  $|\epsilon|$ ,

followed by a sign bit whenever  $\epsilon \neq 0$ , or by using  $G_m(M(\epsilon))$ , where

$$M(\epsilon) = 2|\epsilon| - u(\epsilon) \quad (5)$$

and the indicator function  $u(\epsilon) = 1$  if  $\epsilon < 0$ , or 0 otherwise. Codes of the first type are not used in LOCO-I/JPEG-LS, and are not discussed further in this paper. Instead, we focus on the mapping  $M(\epsilon)$ , which gives the index of  $\epsilon$  in the interleaved sequence  $0, -1, 1, -2, 2, \dots$ . This mapping was first used by Rice in [39] to encode TSGDs centered at zero, by applying a GPO2 code to  $M(\epsilon)$ . Notice that  $M(\epsilon)$  is a very natural mapping under the assumption  $s \leq 1/2$ , since it sorts prediction residuals in nonincreasing order of probability. The corresponding mapping for  $s > 1/2$  is  $M'(\epsilon) = M(-\epsilon - 1)$ , which effects the probability sorting in this case. Following the modular reduction described in Section III-B1, for  $-\lceil \alpha/2 \rceil \leq \epsilon \leq \lceil \alpha/2 \rceil - 1$ , the corresponding values  $M(\epsilon)$  fall in the range  $0 \leq M(\epsilon) \leq \alpha - 1$ . This is also the range for  $M'(\epsilon)$  with even  $\alpha$ . For odd  $\alpha$ ,  $M'(\epsilon)$  can also take on the value  $\alpha$  (but not  $\alpha - 1$ ).

## 2) Sequential Parameter Estimation:

*Statement of the Problem:* Even though, in general, adaptive strategies are easier to implement with arithmetic codes, the family of codes of [35] provides a reasonable alternative for low complexity adaptive coding of TSGDs, which is investigated in [33]: Based on the past sequence of prediction residuals  $\epsilon^t = \epsilon_1 \epsilon_2 \dots \epsilon_t$  encoded at a given context, select a code (i.e., an optimality region, which includes a Golomb parameter  $m$ ) sequentially, and use this code to encode  $\epsilon_{t+1}$ . (Notice that  $t$  here indexes occurrences of a given context, thus corresponding to the variable  $N$  introduced in Section III-B3.) The decoder makes the same determination, after decoding the same past sequence. Thus, the coding is done “on the fly,” as with adaptive arithmetic coders. Two adaptation approaches are possible for selecting the code for  $\epsilon_{t+1}$ : *exhaustive search* of the code that would have performed best on  $\epsilon^t$ , or expected code length minimization for an *estimate* of the TSGD parameters given  $\epsilon^t$ . These two approaches also apply in a *block coding* framework,<sup>7</sup> with the samples in the block to be encoded used in lieu of  $\epsilon^t$ .

An advantage of the estimation approach is that, if based on ML, it depends only on the *sufficient statistics*  $S_t$  and  $N_t$  for the parameters  $\theta$  and  $s$ , given by

$$S_t = \sum_{i=1}^t (|\epsilon_i| - u(\epsilon_i)), \quad N_t = \sum_{i=1}^t u(\epsilon_i)$$

with  $u(\cdot)$  as in (5). Clearly,  $N_t$  is the total number of negative samples in  $\epsilon^t$ , and  $S_t + N_t$  is the accumulated sum of absolute values. In contrast, an exhaustive search would require one counter per context for each code in the family.

*Code Family Reduction:* Despite the relative simplicity of the codes, the complexity of both the code determination and the encoding procedure for the full family of optimal codes of [35] would still be beyond the constraints set for JPEG-LS. For that reason, as in [39], LOCO-I/JPEG-LS only uses the subfamily of

<sup>7</sup>For block coding, an image is divided into rectangular blocks of samples. The blocks are scanned to select a code within a small family, which is identified with a few overhead bits, and the samples are encoded in a second pass through the block (see, e.g., [39]).

GPO2 codes. Furthermore, only codes based on the mappings  $M(\cdot)$  and  $M'(\cdot)$  (for  $s \leq 1/2$  and  $s > 1/2$ , respectively) are used. We denote  $\Gamma_k(\epsilon) = G_{2^k}(M(\epsilon))$ . The mapping  $M'(\cdot)$  is relevant only for  $k = 0$ , since  $\Gamma_k(\epsilon) = \Gamma_k(-\epsilon - 1)$  for every  $k > 0$ . Thus, the sequential code selection process in LOCO-I/JPEG-LS consists of the selection of a Golomb parameter  $k$ ,<sup>8</sup> and in case  $k = 0$ , a mapping  $M(\cdot)$  or  $M'(\cdot)$ . We further denote  $\Gamma'_0(\epsilon) = G_1(M'(\epsilon))$ .

The above subfamily of codes, which we denote  $\mathcal{C}$ , represents a specific compression-complexity trade-off. It is shown in [35] that the average code length with the best code in  $\mathcal{C}$  is within about 4.7% of the optimal prefix codes for TSGDs, with largest deterioration in the very low entropy region, where a different coding method is needed anyway (see Section III-E). Furthermore, it is shown in [38] that the gap is reduced to about 1.8% by including codes based on one of the other mappings mentioned above, with a slightly more complex adaptation strategy. These results are consistent with estimates in [39] for the redundancy of GPO2 codes on OSGDs.

The ML estimation approach is used in LOCO-I/JPEG-LS for code selection within the sub-family  $\mathcal{C}$ . It yields the following result, which is proved in [33] and is the starting point for a chain of approximations leading to the very simple adaptation rule used, in the end, in JPEG-LS.

*Theorem 1:* Let  $\phi \triangleq (\sqrt{5} + 1)/2$  (“golden ratio”). Encode  $\epsilon_{t+1}$ ,  $0 \leq t < n$ , according to the following decision rules.

- 1) If  $S_t \leq \phi t$ , compare  $S_t, t - N_t$ , and  $N_t$ . If  $S_t$  is largest, choose code  $\Gamma_1$ . Otherwise, if  $t - N_t$  is largest, choose  $\Gamma_0$ . Otherwise, choose  $\Gamma'_0$ .
- 2) If  $S_t > \phi t$ , choose code  $\Gamma_{k+1}, k \geq 1$ , provided that

$$\frac{1}{\phi^{(2^{-k+1})} - 1} < \frac{S_t}{t} \leq \frac{1}{\phi^{(2^{-k})} - 1}. \quad (6)$$

Let  $\Lambda(\epsilon^n)$  denote the code length resulting from applying this adaptation strategy to the sequence  $\epsilon^n$ . Let  $\Lambda^*(\theta, s)$  denote the minimum expected codeword length over codes in the sub-family  $\mathcal{C}$  for a TSGD with (unknown) parameters  $\theta$  and  $s$ . Then

$$\frac{1}{n} E_{(\theta, s)}[\Lambda(\epsilon^n)] \leq \Lambda^*(\theta, s) + O\left(\frac{1}{n}\right)$$

where  $E_{(\theta, s)}[\cdot]$  denotes expectation under  $\theta$  and  $s$ .

Theorem 1 involves the decision regions derived in [35, Lemma 4] for  $\mathcal{C}$  in the case of *known* parameters, after *reparameterization* to  $S \triangleq \theta/(1 - \theta)$  and  $\rho \triangleq \theta^{1-s}/(\theta^{1-s} + \theta^s)$ . The (transformed) parameters  $S$  and  $\rho$  are replaced by their (simple) estimates  $S_t/t$  and  $N_t/t$ , respectively. The claim of the theorem applies in a probabilistic setting, in which it is postulated that the data is TSG-distributed with parameters that are unknown to the coders. It states that a sequential adaptation strategy based on ML estimation of the TSGD parameters, and a partition of the parameter space into decision regions corresponding to codes in  $\mathcal{C}$  with minimum expected code length, performs essentially as well (up to an  $O(1/n)$  term) as the best code in  $\mathcal{C}$  for the *unknown* parameters.

<sup>8</sup>We will refer to  $k$  also as a *Golomb parameter*, the distinction from  $2^k$  being clear from the context.

Theorem 1 formalizes related results presented in [39] for block coding. A result analogous to Theorem 1 is proved in [24] for the exhaustive search approach, under a OSGD assumption. There, the deviation from optimality is bounded as  $O(1/\sqrt{n})$ , and the derivation also involves the golden ratio. Notice that the exhaustive search adaptation approach is recommended in both [24] and [39] for selecting GPO2 codes, even though both mention ways of explicitly estimating the parameter  $k$  from observed error values. In [39], an estimation formula based on a sum  $F_0$  over values  $\epsilon$  in a block is presented. The parameter  $k$  is determined according to ranges of values of  $F_0$ . Reference [24] briefly mentions the possibility of deriving  $k$  by first estimating the variance of the distribution from  $\epsilon^t$ . Approximating the sufficient statistics, rather than computing the variance or the sum  $F_0$ , results in a surprisingly simple calculation for  $k$  and, in case  $k = 0$ , also for the mapping.

Next, we present (in two stages) the chain of approximations leading to the adaptation rule used in JPEG-LS.

*First Approximation:* The decision region boundaries (6) admit a low complexity approximation, proposed in [33], for which it is useful to define the functions  $S(k)$  and  $\gamma(k)$ ,  $k > 0$ , by

$$S(k) \triangleq \frac{1}{\phi^{(2^{-k+1})} - 1} \triangleq \frac{2^{k-1}}{\ln \phi} - \frac{1}{2} + \gamma(k). \quad (7)$$

It can be shown that  $\gamma(k)$  is a *decreasing* function of  $k$ , that ranges between  $\phi + (1/2) - (1/\ln \phi) \approx 0.04$  ( $k = 1$ ), and 0 ( $k \rightarrow \infty$ ). Since  $\phi \approx 1.618$  and  $1/\ln \phi \approx 2.078$ , (7) implies that  $S(k)$  is within 4% of  $2^k - (1/2) + (1/8)$  for every  $k > 0$ . Thus, using approximate values of  $S(k)$  and  $S(k+1)$  in lieu of the bounds in (6), a good approximation to the decision rule of Theorem 1 for encoding  $\epsilon_{t+1}$  is as follows.

Let  $S'_t = S_t + (t/2) - (t/8)$ .

- 1) If  $S'_t \leq 2t$ , compare  $S_t, N_t$ , and  $t - N_t$ . If  $S_t$  is largest, choose code  $\Gamma_1$ . Otherwise, if  $t - N_t$  is largest, choose  $\Gamma_0$ . Otherwise, choose  $\Gamma'_0$ .
- 2) If  $S'_t > 2t$ , choose code  $\Gamma_{k+1}$ ,  $k \geq 1$ , provided that  $t2^k \leq S'_t < t2^{k+1}$ .

*Adaptation Rule in JPEG-LS:* The rule used in JPEG-LS further simplifies this approximation. For each context, the accumulated sum of magnitudes of prediction residuals,  $S_t + N_t$ , is maintained in a register  $A$ , in addition to the variables  $B$  and  $N$  defined in Section III-B3. The following procedure is implemented.

- a) Compute  $k$  as

$$k = \min\{k' \mid 2^{k'} N \geq A\}. \quad (8)$$

- b) If  $k > 0$ , choose code  $\Gamma_k$ . Otherwise, if  $k = 0$  and  $2B > -N$ , choose code  $\Gamma_0$ . Otherwise, choose code  $\Gamma'_0$ .

In the above procedure,  $S'_t$  is approximated by  $A$  (implying the assumption that  $N_t$  is reasonably close to  $(t/2) - (t/8)$ ). Values of  $k \geq 2$  in (8) correspond to Step 2) above, while a value  $k = 1$  corresponds to the case where  $S_t$  is largest in Step 1), through the approximation  $N_t \approx t/2$ . The other cases of Step 1) correspond to  $k = 0$ , where a finer approximation of  $N_t$  is used. Recall that  $-B/N$  is an estimate of  $s$ . Clearly,  $s < 1/2$  if

and only if  $\Pr\{\epsilon < 0\} < 1/2$ . Therefore, the result of the comparison  $2B > -N$  approximates the result of the comparison  $2N_t < t$  reasonably well, and the simplified procedure follows.

In software,  $k$  can be computed by the C programming language “one-liner”

```
for (k = 0; (N << k) < A; k++);
```

Hardware implementations are equally trivial.

3) *Limited-Length Golomb Codes:* The encoding procedure of Section III-C can produce significant expansion for single samples: for example, with  $\alpha = 256$  and  $k = 0$ , a prediction residual  $\epsilon = -128$  would produce 256 output bits, a 32:1 expansion. Moreover, one can create artificial images with long sequences of different contexts, such that this situation occurs sample after sample, thus causing significant local expansion (this context pattern is necessary for this situation to arise, as large residuals would otherwise trigger adaptation of  $k$  to a larger value for a particular context). While such a worst-case sequence is not likely in practical situations, significant local expansion was observed for some images. In general, local expansion does not affect the overall compression ratio, as the average or asymptotic expansion behavior is governed by the adaptation of the code parameter  $k$ . However, local expansion can be problematic in implementations with limited buffer space for compressed data. Therefore, adopting a practical tradeoff, GPO2 codes are modified in JPEG-LS to limit the code length per sample to (typically)  $4\beta$ , where  $\beta \triangleq \lceil \log \alpha \rceil$ , e.g., 32 bits for 8-bit/sample images.

The limitation is achieved using a simple technique [6] that avoids a negative impact on complexity, while on the other hand saving, in some situations, the significant cost of outputting long unary representations. For a maximum code word length of  $L_{\max}$  bits, the encoding of an integer  $y$ ,  $0 \leq y \leq \alpha$ ,<sup>9</sup> proceeds as in Section III-C1 whenever  $q(y) = \lfloor 2^{-k}y \rfloor$  satisfies

$$q(y) < L_{\max} - \beta - 1 \triangleq q_{\max} \quad (9)$$

where we assume  $L_{\max} > \beta + 1$ . The case where (9) holds is by far the most frequent, and checking the condition adds only one comparison per encoding. By (8)

$$k \leq \lceil \log \lceil \alpha/2 \rceil \rceil \leq \beta - 1 \quad (10)$$

so that the total code length after appending  $k$  bits is within the required limit  $L_{\max}$ . Now, if  $q(y) \geq q_{\max}$ ,  $q_{\max}$  is encoded in unary, which acts as an “escape” code, followed by an explicit binary representation of  $y - 1$ , using  $\beta$  bits (since  $y = 0$  always satisfies (9), so that  $0 \leq y - 1 < \alpha$ ), for a total of  $L_{\max}$  bits. Although the terminating bit of the unary representation is superfluous, as  $q_{\max}$  zeroes would already identify an escape code, it facilitates the decoding operation.

#### D. Resets

To enhance adaptation to nonstationarity of image statistics, LOCO-I/JPEG-LS periodically resets the variables  $N$ ,  $A$ , and  $B$ . Specifically, we *half* (rounding down to nearest integer) the

<sup>9</sup>Notice that the range for  $y$  may include  $\alpha$  in case  $\alpha$  is odd and the mapping  $M(\cdot)$  is used.



contents of  $N$ ,  $A$ , and  $B$  for a given context each time  $N$  attains a predetermined threshold  $N_0$ . In this way, the immediate past is given a larger weight than the remote past. It has been found that values of  $N_0$  between 32 and 256 work well for typical images; the default value in JPEG-LS is 64. More importantly in practice, resetting the variables limits the amount of storage required per context.

### E. Embedded Alphabet Extension (Run Coding)

*Motivation:* Symbol-by-symbol (Huffman) coding (as opposed to arithmetic coding) is inefficient for very low entropy distributions, due to its fundamental limitation of producing at least one code bit per encoding. This limitation applies to the symbol-by-symbol coding of TSGDs performed in LOCO-I/JPEG-LS, and may produce a significant redundancy (i.e., excess code length over the entropy) for contexts representing smooth regions, for which the distributions are very peaked as a prediction residual of 0 is extremely likely. In nonconditioned codes, this problem is addressed through *alphabet extension*. By encoding blocks of data as “super-symbols,” distributions tend to be flatter (i.e., the redundancy is spread over many symbols).

*Mode Selection:* A strategy similar to the above has been embedded into the context model in LOCO-I/JPEG-LS. The encoder enters a “run” mode when a “flat region” context with  $a = b = c = d$  is detected. Since the central region of quantization for the gradients  $g_1, g_2, g_3$  is the singleton  $\{0\}$ , the run condition is easily detected in the process of context quantization by checking for  $[q_1, q_2, q_3] = [0, 0, 0]$ . Once in run mode, a run of the symbol  $a$  is expected, and the run length (which may be zero) is encoded. While in run mode, the context is not checked and some of the samples forming the run may occur in contexts other than  $[0, 0, 0]$ . When the run is broken by a non-matching sample  $x$ , the encoder goes into a “run interruption” state, where the difference  $\epsilon = x - b$  (with the sample above  $x$ ) is encoded. Runs can also be broken by ends of lines, in which case the encoder returns to normal context-based coding. Since all the decisions for switching in and out of the run mode are based on past samples, the decoder can reproduce the same decisions without any side information.

*Adaptive Run Length Coding:* The encoding of run lengths in JPEG-LS is also based on Golomb codes, originally proposed in [32] for such applications. However, an improved adaptation strategy can be derived from viewing the encoded sequence as binary (“0” for a “hit,” “1” for a “miss”). For a positive integer parameter  $m$ , let  $EG_m$  denote a variable-to-variable length code defined over the extended binary alphabet  $\{1, 01, 001, \dots, 0^{m-1}1, 0^m\}$ , where  $0^\ell$  denotes a sequence of  $\ell$  zeros. Under  $EG_m$ , the extended symbol  $0^m$  (a successful run of  $m$  “hits”) is encoded with a 0, while  $0^\ell 1$ ,  $0 \leq \ell < m$ , is encoded with a 1 followed by the modified binary representation of  $\ell$ . By considering a concatenation of extended input symbols, it is easy to see that  $EG_m$  is equivalent to  $G_m$  applied to the run length. However,  $EG_m$  is defined over a finite alphabet, with “hits” and “misses” modeled as independent and identically distributed (i.i.d.). We will refer to  $EG_m$  as an *elementary Golomb code* of order  $m$ . Variations

of these codes were introduced in [36], [43], and [44] in the context of adaptive run-length coding. They are also studied in [45] in the context of embedded coding of wavelet coefficients, where insight is provided into their well-known efficiency for encoding i.i.d. binary sequences over a surprisingly wide range of values of the probability  $q$  of a zero.

When  $q$  is unknown *a priori*, elementary Golomb codes are superior to Golomb codes in that the value of  $m$  can be adapted *within a run*, based on the current estimate of  $q$ . The optimal adaptation turns out to be extremely simple if the family of codes is reduced, again, to the case  $m = 2^g$ , while the redundancy remains very small for the ranges of interest. In addition, the code words for interrupted runs are all  $g + 1$  bits long and provide explicitly the length of the interrupted run. This approach, proposed in [2], was adopted in JPEG-LS and replaces the approach used in [1]. It is inspired in [36], and is termed *block-MEL-CODE*.

Count-based adaptation strategies for the parameter  $g$  are proposed in [36] and [45]. JPEG-LS uses a predefined table to approximate these strategies. A run segment of length  $m$  (i.e.,  $0^m$ ) triggers an index increment, while a “miss” (i.e.,  $0^\ell 1$ ,  $0 \leq \ell < m$ ) triggers an index decrement. The index is used to enter the table, which determines how many consecutive run segments (resp. “misses”) trigger an increment (resp. decrement) of  $g$  (see [7]).

*Run Interruption Coding:* The coding procedure for a run interruption sample  $x$  is applied to  $\epsilon = x - b \bmod \alpha$ . Thus, both the fixed predictor (1) and the bias cancellation procedure are skipped. Coding is otherwise similar to the regular sample case. However, conditioning is based on two special contexts, determined according to whether  $a = b$  or  $a \neq b$ . In the former case, we always have  $\epsilon \neq 0$  (since, by definition of run interruption,  $x \neq a$ ). Therefore, the mappings  $M(\cdot)$  and  $M'(\cdot)$  are modified to take advantage of this exclusion. Moreover, since the  $B$  counter is not used in these contexts (no bias cancellation is performed), the decision between  $M(\cdot)$  and  $M'(\cdot)$  is based on the number  $N_t$  of negative values occurring in each context. The same reset procedure as in Section III-D is used for the corresponding counters. Also, the length limitation for the Golomb code takes into account the  $g + 1$  bits of the last coded run segment, thus limiting every code word length to  $L_{\max} - g - 1$  bits.

### F. Summary of Encoding Procedures

Figs. 4 and 5 summarize the JPEG-LS lossless encoding procedures for a single component of an image. The decoding process uses the same basic procedures and follows almost the same steps in reverse order (see [7] for details). Undefined samples in the causal template at the boundaries of the image are treated as follows: For the first line,  $b = c = d = 0$  is assumed. For the first and last column, whenever undefined, the samples at positions  $a$  and  $d$  are assumed to be equal to the one at position  $b$ , while the value of the samples at position  $c$  is copied from the value that was assigned to position  $a$  when encoding the first sample in the previous line.

For ease of cross-reference, for the main steps of the procedures in Fig. 4 we indicate, in square brackets, the label of the corresponding block in Fig. 1, and the numbers of the sub-sections where the computation is discussed. Fig. 5 corresponds to

- Step 0.** Initialization:
- Compute  $L_{\max} = 2(\beta_{\max} + \max\{8, \beta_{\max}\})$ , where  $\beta_{\max} = \max\{2, \lceil \log \alpha \rceil\}$ .
  - Initialize the 365 sets of context counters  $A$ ,  $B$ ,  $C$ , and  $N$  as follows:  $B = C = 0$ ,  $N = 1$ ,  $A = \max\{2, \lceil (\alpha + 32)/64 \rceil\}$ . Similar initializations are needed for the corresponding variables in the two run interruption contexts.
  - Initialize to 0 the index  $I_{\text{RUN}}$  to the run mode adaptation table.
  - Set current sample  $x$  to the first sample in the image.
- Step 1.** Compute the “local gradients”  $g_1 = d - b$ ,  $g_2 = b - c$ , and  $g_3 = c - b$ . [Gradients, III-B2]
- Step 2.** If  $g_1 = g_2 = g_3 = 0$ , go to run mode processing (Fig. 5). Otherwise, continue in “regular” mode. [Flat Region?, III-E]
- Step 3.** Quantize the local gradients  $g_i$ ,  $i = 1, 2, 3$ . [Context Modeler, III-B2]
- Step 4.** Denote the quantized gradients by  $q_i$ ,  $i = 1, 2, 3$ . If the first non-zero component of  $\{q_1, q_2, q_3\}$  is negative, reverse all the signs in the triplet and associate a negative sign to it. Otherwise, associate a positive sign. Map the triplet, on a one-to-one basis, into an index in the range  $[1, 364]$  (context number 0 is reserved to the run mode). Use the index to address the context counters. [Context Modeler, III-B2]
- Step 5.** Compute the fixed prediction  $\hat{x}_{\text{MED}}$  according to (1). [Fixed Predictor, III-A]
- Step 6.** Correct  $\hat{x}_{\text{MED}}$  by adding (resp. subtracting) the value of  $C$  for the context in case the sign associated to the context is positive (resp. negative). Clamp the corrected value to the range  $[0, \alpha - 1]$  to obtain the corrected prediction  $\hat{x}$ . [Adaptive Correction, III-B3]
- Step 7.** Compute the prediction residual  $\bar{\epsilon} = x - \hat{x}$  and, if a negative sign is associated to the context, set  $\bar{\epsilon} \leftarrow -\bar{\epsilon}$ . Reduce  $\bar{\epsilon}$  modulo  $\alpha$  to a value  $\epsilon$  in the range  $[-\lceil \alpha/2 \rceil, \lceil \alpha/2 \rceil - 1]$ . [subtractor  $\ominus$ , III-B1, III-B2]
- Step 8.** Compute the Golomb parameter  $k$  according to (8). [Context Modeler, III-C2]
- Step 9.** Map  $\epsilon$  to  $M(\epsilon)$  or, if  $k = 0$  and  $2B \leq -N$ , to  $M'(\epsilon)$ . [Context Modeler, III-C2]
- Step 10.** Golomb-encode the mapped prediction residual using the parameter  $k$  and, if necessary, perform the code word length limitation procedure with maximum length  $L_{\max}$ . [Golomb Coder, III-C1, III-C3]
- Step 11.** Update the context counters by adding  $\epsilon$  to  $B$  and  $|\epsilon|$  to  $A$ , halving  $A$ ,  $B$ , and  $N$  in case  $N = N_0$  (reset threshold), and incrementing  $N$ . [Context Modeler, III-C2, III-D]
- Step 12.** Update the values of  $B$  and  $C$  following the “if-else” statement in Figure 3. [Context Modeler, III-B3]
- Step 13.** Go to Step 1 to process the next sample.

Fig. 4. JPEG-LS: Encoding of a single component.

- Step 1.** Read new samples until either  $x \neq a$  or the end of the line is encountered.
- Step 2.** Let  $m = 2^g$  denote the current parameter of the elementary Golomb code. For each run segment of length  $m$ , append a ‘1’ to the output bit stream and increment the index  $I_{\text{RUN}}$ . If so indicated by the table, double  $m$ .
- Step 3.** If the run was interrupted by the end of a line, append ‘1’ to the output bit stream and go to Step 1 of the main algorithm (Fig. 4). Otherwise, append ‘0’ to the output bit stream followed by the binary representation of the residual run length using  $g$  bits, decrement  $I_{\text{RUN}}$ , and if so indicated by the table, half  $m$ .
- Step 4.** Encode the run interruption sample and go to Step 1 of the main algorithm (Fig. 4).

Fig. 5. JPEG-LS: Run mode processing.

the blocks labeled “Run Counter” and “Run Coder” discussed in Section III-E.

#### IV. NEAR-LOSSLESS COMPRESSION

JPEG-LS offers a lossy mode of operation, termed “near-lossless,” in which every sample value in a reconstructed image component is guaranteed to differ from the corresponding value in the original image by up to a preset (small) amount,  $\delta$ . The basic technique employed for achieving this goal is the traditional DPCM loop [21], where the prediction residual (after correction and possible sign reversion, but before modulo reduction) is quantized into quantization bins of size  $2\delta + 1$ , with

reproduction at the center of the interval. Quantization of a prediction residual  $\epsilon$  is performed by integer division according to

$$Q(\epsilon) = \text{sign}(\epsilon) \left\lfloor \frac{|\epsilon| + \delta}{2\delta + 1} \right\rfloor. \quad (11)$$

Since  $\delta$  usually takes one of a few small integer values, the integer division in (11) can be performed efficiently both in hardware [46] and software (e.g., with look-up tables).

The following aspects of the coding procedure are affected by the quantization step. Context modeling and prediction are based on reconstructed values, so that the decoder can mimic the operation of the encoder. In the sequel, the notation  $a, b, c$ , and  $d$ , will be used to refer also to the reconstructed values of the samples at these positions. The condition for entering the

run mode is relaxed to require that the gradients  $g_i, i = 1, 2, 3$ , satisfy  $|g_i| \leq \delta$ . This relaxed condition reflects the fact that reconstructed sample differences up to  $\delta$  can be the result of quantization errors. Moreover, once in run mode, the encoder checks for runs within a tolerance of  $\delta$ , while reproducing the value of the reconstructed sample at  $a$ . Consequently, the two run interruption contexts are determined according to whether  $|a - b| \leq \delta$  or not.

The relaxed condition for the run mode also determines the central region for quantized gradients, which is  $|g_i| \leq \delta, i = 1, 2, 3$ . Thus, the size of the central region is increased by  $2\delta$ , and the default thresholds for gradient quantization are scaled accordingly.

The reduction of the quantized prediction residual is done modulo  $\alpha'$ , where

$$\alpha' = \left\lfloor \frac{\alpha + 4\delta}{2\delta + 1} \right\rfloor$$

into the range  $[-\lfloor \alpha'/2 \rfloor, \lceil \alpha'/2 \rceil - 1]$ . The reduced value is (losslessly) encoded and recovered at the decoder, which first multiplies it by  $2\delta + 1$ , then adds it to the (corrected) prediction (or subtracts it, if the sign associated to the context is negative), and reduces it modulo  $\alpha'(2\delta + 1)$  into the range  $[-\delta, \alpha' \cdot (2\delta + 1) - 1 - \delta]$ , finally clamping it into the range  $[0, \alpha - 1]$ . It can be seen that, after modular reduction, the recovered value cannot be larger than  $\alpha - 1 + \delta$ . Thus, before clamping, the decoder actually produces a value in the range  $[-\delta, \alpha - 1 + \delta]$ , which is precisely the range of possible sample values with an error tolerance of  $\pm\delta$ .

As for encoding,  $\alpha'$  replaces  $\alpha$  in the definition of the limited-length Golomb coding procedure. Since  $A$  accumulates quantized error magnitudes,  $k < \lceil \log \alpha' \rceil$ . On the other hand,  $B$  accumulates the encoded value, *multiplied* by  $2\delta + 1$ . The alternative mapping  $M'(\cdot)$  is not used, as its effect would be negligible since the center of the quantized error distribution is in the interval  $(-1/(2\delta + 1), 0]$ .

The specification [7] treats the lossless mode as a special case of near-lossless compression, with  $\delta = 0$ . Although the initial goal of this mode was to guarantee a bounded error for applications with legal implications (e.g., medical images), for small values of  $\delta$  its visual and SNR performance is often superior to that of traditional transform coding techniques [49].

## V. VARIATIONS ON THE BASIC CONFIGURATION

### A. Lower Complexity Variants

The basic ideas behind LOCO-I admit variants that can be implemented at an even lower complexity, with reasonable deterioration in the compression ratios. One such variant follows from further applying the principle that prior knowledge on the structure of images should be used, whenever available, thus saving model learning costs (see Section II-A). Notice that the value of the Golomb parameter  $k$  is (adaptively) estimated at each context based on the value of previous prediction residuals. However, the value of  $k$  for a given context can be generally estimated *a priori*, as “active” contexts, corresponding to larger gradients, will tend to present flatter distributions. In fact, for most contexts there is a strong correlation between the “activity

level” measure  $|d - b| + |b - c| + |c - a|$ , and the value of  $k$  that ends up being used the most in the context, with larger activity levels corresponding to larger values of  $k$ . However, the quantization threshold for the activity level would strongly depend on the image.

The above observation is related to an alternative interpretation of the modeling approach in LOCO-I.<sup>10</sup> Under this interpretation, the use of only  $|C|$  different prefix codes to encode context-dependent distributions of prediction residuals, is viewed as a (dynamic) way of clustering conditioning contexts. The clusters result from the use of a small family of codes, as opposed to a scheme based on arithmetic coding, which would use different arithmetic codes for different distributions. Thus, this aspect of LOCO-I can also be viewed as a realization of the basic paradigm proposed and analyzed in [12] and also used in CALIC [17], in which a multiplicity of predicting contexts is clustered into a few conditioning states. In the lower complexity alternative proposed in this section, the clustering process is static, rather than dynamic. Such a static clustering can be obtained, for example, by using the above activity level in lieu of  $A$ , and  $N = 3$ , to determine  $k$  in (8).

### B. LOCO-A: An Arithmetic Coding Extension

In this section, we present an arithmetic coding extension of LOCO-I, termed LOCO-A [47], which has been adopted for a prospective extension of the baseline JPEG-LS standard (JPEG-LS Part 2). The goal of this extension is to address the basic limitations that the baseline presents when dealing with very compressible images (e.g., computer graphics, near-lossless mode with an error of  $\pm 3$  or larger), due to the symbol-by-symbol coding approach, or with images that are very far from being continuous-tone or have sparse histograms. Images of the latter type contain only a subset of the possible sample values in each component, and the fixed predictor (1) would tend to concentrate the value of the prediction residuals into a reduced set. However, prediction correction tends to spread these values over the entire range, and even if that were not the case, the probability assignment of a TSGD model in LOCO-I/JPEG-LS would not take advantage of the reduced alphabet.

In addition to better handling the special types of images mentioned above, LOCO-A closes, in general, most of the (small) compression gap between JPEG-LS and the best published results (see Section VI), while still preserving a certain complexity advantage due to simpler prediction and modeling units, as described below.

LOCO-A is a natural extension of the JPEG-LS baseline, requiring the same buffering capability. The context model and most of the prediction are identical to those in LOCO-I. The basic idea behind LOCO-A follows from the alternative interpretation of the modeling approach in LOCO-I discussed in Section V-A. There, it was suggested that *conditioning states* could be obtained by clustering contexts based on the value of the Golomb parameter  $k$  (thus grouping contexts with similar conditional distributions). The resulting state-conditioned distributions can be arithmetic encoded, thus relaxing the TSGD assumption, which would thus be used only as a means to form

<sup>10</sup>X. Wu, private communication.

the states. The relaxation of the TSGD assumption is possible due to the small number of states,  $|C| = \lceil \log \alpha \rceil + 1$ , which enables the modeling of more parameters per state. In LOCO-A, this idea is generalized to create higher resolution clusters based on the average magnitude  $A/N$  of prediction residuals (as  $k$  is itself a function of  $A/N$ ). Since, by definition, each cluster would include contexts with very similar conditional distributions, this measure of activity level can be seen as a refinement of the “error energy” used in CALIC [17], and a further application of the paradigm of [12]. Activity levels are also used in the ALCM algorithm [48].

Modeling in LOCO-A proceeds as in LOCO-I, collecting the same statistics at each context (the “run mode” condition is used to define a separate encoding state). The clustering is accomplished by modifying (8) as follows:

$$k = \min\{k' \mid 2^{k'/2}N \geq A\}.$$

For 8-bit/sample images, 12 encoding states are defined:  $k = 0, k = 1, \dots, k = 9, k > 9$ , and the run state. A similar clustering is possible with other alphabet sizes.

Bias cancellation is performed as in LOCO-I, except that the correction value is tuned to produce TSGDs with a shift  $s$  in the range  $-1/2 \leq s < 1/2$ , instead of  $0 \leq s < 1$  (as the coding method that justified the negative fractional shift in LOCO-I is no longer used). In addition, regardless of the computed correction value, the corrected prediction is incremented or decremented in the direction of  $\hat{x}_{\text{MED}}$  until it is either a value that has already occurred in the image, or  $\hat{x}_{\text{MED}}$ . This modification alleviates the unwanted effects on images with sparse histograms, while having virtually no effect on “regular” images. No bias cancellation is done in the run state. A “sign flip” borrowed from the CALIC algorithm [17] is performed: if the bias count  $B$  is positive, then the sign of the error is flipped. In this way, when distributions that are similar in shape but have opposite biases are merged, the statistics are added “in phase.” Finally, prediction errors are arithmetic-coded conditioned on one of the 12 encoding states. Binary arithmetic coding is performed, following the Golomb-based binarization strategy of [48]. For a state with index  $k$ , we choose the corresponding binarization tree as the Golomb tree for the parameter  $2^{\lceil k/2 \rceil}$  (the run state also uses  $k = 0$ ).

Note that the modeling complexity in LOCO-A does not differ significantly from that of LOCO-I. The only added complexity is in the determination of  $k$  (which, in software, can be done with a simple modification of the C “one-liner” used in LOCO-I), in the treatment of sparse histograms, and in the use of a fifth sample in the causal template, West of  $a$ , as in [1]. The coding complexity, however, is higher due to the use of an arithmetic coder.

## VI. RESULTS

In this section, we present compression results obtained with the basic configuration of JPEG-LS discussed in Section III, using default parameters in separate single-component scans. These results are compared with those obtained with other relevant schemes reported in the literature, over a wide variety of images. We also present results for near-lossless compression

TABLE I  
COMPRESSION RESULTS ON ISO/IEC  
10918-1 IMAGE TEST SET (IN BITS/SAMPLE)

Image	LOCO-I	JPEG-LS	$\delta=1$	$\delta=3$
Balloon	2.68	2.67	1.50	0.88
Barb 1	3.88	3.89	2.45	1.59
Barb 2	3.99	4.00	2.56	1.65
Board	3.20	3.21	1.83	0.98
Boats	3.34	3.34	1.98	1.14
Girl	3.39	3.40	2.03	1.28
Gold	3.92	3.91	2.46	1.52
Hotel	3.78	3.80	2.36	1.45
Zelda	3.35	3.35	1.97	1.21
Average	3.50	3.51	2.13	1.30

and for LOCO-A. Compression ratios are given in bits/sample.<sup>11</sup>

In Table I, we study the compression performance of LOCO-I and JPEG-LS in lossless mode, as well as JPEG-LS in near-lossless mode with  $\delta = 1$  and  $\delta = 3$ , on a standard set of images used in developing the JPEG standard [20]. These are generally “smooth” natural images, for which the  $U$  and  $V$  components have been down-sampled 2 : 1 in the horizontal direction. The LOCO-I column corresponds to the scheme described in [1], and the discrepancy with the JPEG-LS column reflects the main differences between the algorithms, which in the end cancel out. These differences include: use of a fifth context sample in LOCO-I, limitation of Golomb code word lengths in JPEG-LS, different coding methods in run mode, different treatment of the mapping  $M'(\cdot)$ , and overhead in JPEG-LS due to the more elaborate data format (e.g., marker segments, bit stuffing, etc.).

Notice that, assuming a uniform distribution for the quantization error, the root mean square error (RMSE) per component for a maximum loss  $\delta$  in near-lossless mode would be

$$\text{RMSE} = \sqrt{\frac{2 \sum_{i=1}^{\delta} i^2}{2\delta + 1}}. \quad (12)$$

In practice, this estimate is accurate for  $\delta = 1$  (namely,  $\text{RMSE} \approx 0.816$ ), while for  $\delta = 3$  the actual RMSE (an average of 1.94 for the images in Table I) is slightly better than the value  $\text{RMSE} = 2$  estimated in (12). For such small values of  $\delta$ , the near-lossless coding approach is known to largely outperform the (lossy) JPEG algorithm [20] in terms of RMSE at similar bit-rates [49]. For the images in Table I, typical RMSE values achieved by JPEG at similar bit-rates are 1.5 and 2.3, respectively. On these images, JPEG-LS also outperforms the emerging wavelet-based JPEG 2000 standard [50] in terms of RMSE for bit-rates corresponding to  $\delta = 1$ .<sup>12</sup> At bit-rates corresponding to  $\delta > 2$ , however, the wavelet-based scheme yields far better RMSE. On the other hand, JPEG-LS is considerably simpler and guarantees a maximum per-sample error, while JPEG 2000 offers other features.

<sup>11</sup>The term “bits/sample” refers to the number of bits in each component sample. Compression ratios will be measured as the total number of bits in the compressed image divided by the total number of samples in all components, after possible down-sampling.

<sup>12</sup>The default (9, 7) floating-point transform was used in these experiments, in the so-called “best mode” (non-SNR-scalable). The progressive-to-lossless mode (reversible wavelet transform) yields worse results even at bit-rates corresponding to  $\delta = 1$ .

TABLE II  
COMPRESSION RESULTS ON NEW IMAGE TEST SET (IN BITS/SAMPLE)

Image	LOCO-I	JPEG-LS	FELICS	Lossless JPEG Huffman	Lossless JPEG arithm.	CALIC arithm.	LOCO-A	PNG
bike	3.59	3.63	4.06	4.34	3.92	3.50	3.54	4.06
cafe	4.80	4.83	5.31	5.74	5.35	4.69	4.75	5.28
woman	4.17	4.20	4.58	4.86	4.47	4.05	4.11	4.68
tools	5.07	5.08	5.42	5.71	5.47	4.95	5.01	5.38
bike3	4.37	4.38	4.67	5.18	4.78	4.23	4.33	4.84
cats	2.59	2.61	3.32	3.73	2.74	2.51	2.54	2.82
water	1.79	1.81	2.36	2.63	1.87	1.74	1.75	1.89
finger	5.63	5.66	6.11	5.95	5.85	5.47	5.50	5.81
us	2.67	2.63	3.28	3.77	2.52	2.34	2.45	2.84
chart	1.33	1.32	2.14	2.41	1.45	1.28	1.18	1.40
chart_s	2.74	2.77	3.44	4.06	3.07	2.66	2.65	3.21
compound1	1.30	1.27	2.39	2.75	1.50	1.24	1.21	1.37
compound2	1.35	1.33	2.40	2.71	1.54	1.24	1.25	1.46
aerial2	4.01	4.11	4.49	5.13	4.14	3.83	3.58	4.44
faxballs	0.97	0.90	1.74	1.73	0.84	0.75	0.64	0.96
gold	3.92	3.91	4.10	4.33	4.13	3.83	3.85	4.15
hotel	3.78	3.80	4.06	4.39	4.15	3.71	3.72	4.22
Average	3.18	3.19	3.76	4.08	3.40	3.06	3.06	3.46

Table II shows (lossless) compression results of LOCO-I, JPEG-LS, and LOCO-A, compared with other popular schemes. These include FELICS [24], for which the results were extracted from [17], and the two versions of the original lossless JPEG standard [20], i.e., the strongest one based on arithmetic coding, and the simplest one based on a fixed predictor followed by Huffman coding using “typical” tables [20]. This one-pass combination is probably the most widely used version of the old lossless standard. The table also shows results for PNG, a popular file format in which lossless compression is achieved through prediction (in two passes) and a variant of LZ77 [51] (for consistency, PNG was run in a plane-by-plane fashion). Finally, we have also included the arithmetic coding version of the CALIC algorithm, which attains the best compression ratios among schemes proposed in response to the Call for Contributions leading to JPEG-LS. These results are extracted from [17]. The images in Table II are the subset of 8-bit/sample images from the benchmark set provided in the above Call for Contributions. This is a richer set with a wider variety of images, including compound documents, aerial photographs, scanned, and computer generated images.

The results in Table II, as well as other comparisons presented in [1], show that LOCO-I/JPEG-LS significantly outperforms other schemes of comparable complexity (e.g., PNG, FELICS, JPEG-Huffman), and it attains compression ratios similar or superior to those of higher complexity schemes based on arithmetic coding (e.g., Sunset CB9 [16], JPEG-Arithmetic). LOCO-I/JPEG-LS is, on the average, within a few percentage points of the best available compression ratios (given, in practice, by CALIC), at a much lower complexity level. Here, complexity was estimated by measuring running times of software implementations made widely available by the authors of the compared schemes.<sup>13</sup> The experiments showed a compression time advantage for JPEG-LS over CALIC of about 8:1 on nat-

ural images and significantly more on compound documents. Of course, software running times should be taken very cautiously and only as rough complexity benchmarks, since many implementation optimizations are possible, and it is difficult to guarantee that all tested implementations are equally optimized. However, these measurements do provide a useful indication of relative practical complexity.

As for actual compression speeds in software implementations, LOCO-I/JPEG-LS benchmarks at a throughput similar to that of the UNIX *compress* utility, which is also the approximate throughput reported for FELICS in [24], and is faster than PNG by about a 3 : 1 ratio. Measured compression data rates, for a C-language implementation on a 1998 vintage 300 MHz Pentium II machine, range from about 1.5 MBytes/s for natural images to about 6 MBytes/s for compound documents and computer graphics images. The latter speed-up is due in great part to the frequent use of the run mode. LOCO-I/JPEG-LS decompression is about 10% slower than compression, making it a fairly symmetric system.

Extensive testing on medical images of various types reported in [55] reveals an average compression performance for JPEG-LS within 2.5% of that of CALIC. It is recommended in [55] that the Digital Imaging and Communications in Medicine (DICOM) standard add a transfer syntax for JPEG-LS.

Table II also shows results for LOCO-A. The comparison with CALIC shows that the latter scheme maintains a slight advantage (1–2%) for “smooth” images, while LOCO-A shows a significant advantage for the classes of images it targets: sparse histograms (“aerial2”) and computer-generated (“faxballs”). Moreover, LOCO-A performs as well as CALIC on compound documents without using a separate binary mode [17]. The average compression ratios for both schemes end up equal.

It is also interesting to compare LOCO-A with the JBIG algorithm [52] as applied in [53] to multilevel images (i.e., bit-plane coding of Gray code representation). In [53], the components of the images of Table I are reduced to amplitude precisions below 8 bits/sample, in order to provide data for testing how algorithm performances scale with precision. LOCO-A outper-

<sup>13</sup>The experiments were carried out with JPEG-LS executables available from <http://www.hpl.hp.com/loco>, and CALIC executables available from [ftp://ftp.csd.uwo.ca/pub/from\\_wu](ftp://ftp.csd.uwo.ca/pub/from_wu) as of the writing of this article. A common platform for which both programs were available was used.

forms JBIG for all precisions above 3 bits/sample: for example, at 4 bits/sample (i.e., considering down-sampling, a total of 8 bits/pixel), the average image size for LOCO-A is 1.38 bits/pixel, whereas the average size reported in [53] for JBIG is 1.42 bits/pixel. At 3 bits/sample, the relation is reverted: the averages are 0.86 and 0.83 bits/pixel, respectively. While the JPEG-LS baseline outperforms JBIG by 11% on the average at 8 bits/sample for the images of Table I (the average compressed image size reported in [53] is 3.92 bits/sample), the relative performance deteriorates rapidly below 6 bits/sample, which is the minimum precision for which baseline JPEG-LS still yields better compression ratios (3.68 against 3.87 bits/pixel). Thus, LOCO-A indeed addresses the basic limitations that the baseline presents when dealing with very compressible images.

Software implementations of JPEG-LS for various platforms are available at <http://www.hpl.hp.com/loco/>. The organizations holding patents covering aspects of JPEG-LS have agreed to allow payment-free licensing of these patents for use in the standard.

## APPENDIX

### OTHER FEATURES OF THE STANDARD

*Bit Stream:* The compressed data format for JPEG-LS closely follows the one specified for JPEG [20]. The same high level syntax applies, with the bit stream organized into frames, scans, and restart intervals within a scan, markers specifying the various structural parts, and marker segments specifying the various parameters. New marker assignments are compatible with [20]. One difference, however, is the existence of default values for many of the JPEG-LS coding parameters (e.g., gradient quantization thresholds, reset threshold), with marker segments used to override these values. In addition, the method for easy detection of marker segments differs from the one in [20]. Specifically, a single byte of coded data with the hexadecimal value “FF” is followed with the insertion of a single bit ‘0,’ which occupies the most significant bit position of the next byte. This technique is based on the fact that all markers start with an “FF” byte, followed by a bit “1.”

*Color Images:* For encoding images with more than one component (e.g., color images), JPEG-LS supports combinations of single-component and multicomponent scans. Section III describes the encoding process for a single-component scan. For multicomponent scans, a single set of context counters (namely,  $A$ ,  $B$ ,  $C$ , and  $N$  for regular mode contexts) is used across all components in the scan. Prediction and context determination are performed as in the single component case, and are component independent. Thus, the use of possible correlation between color planes is limited to sharing statistics, collected from all planes. For some color spaces (e.g., RGB), good decorrelation can be obtained through simple lossless color transforms as a pre-processing step to JPEG-LS. For example, compressing the (R-G,G,B-G) representations of the images of Table I, with differences taken modulo the alphabet size  $\alpha$  in the interval  $[-\lfloor\alpha/2\rfloor, \lfloor\alpha/2\rfloor - 1]$ , yields savings between 25% and 30% over compressing the respective RGB representations. These savings are similar to those obtained

with more elaborate schemes which do not assume prior knowledge of the color space [26]. Given the variety of color spaces, the standardization of specific filters was considered beyond the scope of JPEG-LS, and color transforms are handled at the application level.

In JPEG-LS, the data in a multicomponent scan can be interleaved either by lines (*line-interleaved mode*) or by samples (*sample-interleaved mode*). In line-interleaved mode, assuming an image that is not subsampled in the vertical direction, a full line of each component is encoded before starting the encoding of the next line (for images subsampled in the vertical direction, more than one line from a component are interleaved before starting with the next component). The index to the table used to adapt the elementary Golomb code in run mode is component-dependent.

In sample-interleaved mode, one sample from each component is processed in turn, so that all components which belong to the same scan must have the same dimensions. The runs are common to all the components in the scan, with run mode selected only when the corresponding condition is satisfied for *all* the components. Likewise, a run is interrupted whenever so dictated by *any* of the components. Thus, a single run length, common to all components, is encoded. This approach is convenient for images in which runs tend to be synchronized between components (e.g., synthetic images), but should be avoided in cases where run statistics differ significantly across components, since a component may systematically cause run interruptions for another component with otherwise long runs. For example, in a CMYK representation, the runs in the  $K$  plane tend to be longer than in the other planes, so it is best to encode the  $K$  plane in a different scan.

The performance of JPEG-LS, run in line-interleaved mode on the images of Table II, is very similar to that of the component-by-component mode shown in the table. We observed a maximum compression ratio deterioration of 1% on “gold” and “hotel,” and a maximum improvement of 1% on “compound1.” In sample-interleaved mode, however, the deterioration is generally more significant (3% to 5% in many cases), but with a 3% to 4% improvement on compound documents.

*Palletized Images:* The JPEG-LS data format also provides tools for encoding palletized images in an appropriate index space (i.e., as an array of indices to a palette table), rather than in the original color space. To this end, the decoding process may be followed by a so-called *sample-mapping procedure*, which maps each decoded sample value (e.g., an 8-bit index) to a reconstructed sample value (e.g., an RGB triplet) by means of mapping tables. Appropriate syntax is defined to allow embedding of these tables in the JPEG-LS bit stream.

Many of the assumptions for the JPEG-LS model, targeted at continuous-tone images, do not hold when compressing an array of indices. However, an appropriate reordering of the palette table can sometimes alleviate this deficiency. Some heuristics are known that produce good results at low complexity, without using image statistics. For example, [54] proposes to arrange the palette colors in increasing order of luminance value, so that samples that are close in space in a smooth image will tend to be close in color and in luminance. Using this reordering, JPEG-LS outperforms PNG by about 6% on palletized versions of the

images “Lena” and “gold.” On the other hand, PNG may be advantageous for dithered, halftoned, and some graphic images for which LZ-type methods are better suited. JPEG-LS does not specify a particular heuristic for palette ordering.

The sample-mapping procedure can also be used to alleviate the problem of “sparse histograms” mentioned in Section V-B, by mapping the sparse samples to a contiguous set. This histogram compaction, however, assumes a prior knowledge of the histogram sparseness not required by the LOCO-A solution, and is done off-line. The standard extension (JPEG-LS Part 2) includes provisions for on-line compaction with LOCO-I/JPEG-LS.

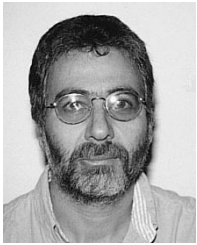
#### ACKNOWLEDGMENT

The authors would like to thank H. Kajiwara, G. Langdon, D. Lee, N. Memon, F. Ono, E. Ordentlich, M. Rabbani, D. Speck, I. Ueno, X. Wu, and T. Yoshida for useful discussions.

#### REFERENCES

- [1] M. J. Weinberger, G. Seroussi, and G. Sapiro, “LOCO-I: A low complexity, context-based, lossless image compression algorithm,” in *Proc. 1996 Data Compression Conference*, Snowbird, UT, Mar. 1996, pp. 140–149.
- [2] *Proposed Modification of LOCO-I for Its Improvement of the Performance*, Feb. 1996. ISO/IEC JTC1/SC29/WG1 Doc. N297.
- [3] *Fine-Tuning the Baseline*, June 1996. ISO/IEC JTC1/SC29/WG1 Doc. N341.
- [4] *Effects of Resets and Number of Contexts on the Baseline*, June 1996. ISO/IEC JTC1/SC29/WG1 Doc. N386.
- [5] *Palettes and Sample Mapping in JPEG-LS*, Nov. 1996. ISO/IEC JTC1/SC29/WG1 Doc. N412.
- [6] *JPEG-LS with Limited-Length Code Words*, July 1997. ISO/IEC JTC1/SC29/WG1 Doc. N538.
- [7] *Information Technology—Lossless and Near-Lossless Compression of Continuous-Tone Still Images*, 1999. ISO/IEC 14495-1, ITU Recommend. T.87.
- [8] *LOCO-I: A Low Complexity Lossless Image Compression Algorithm*, July 1995. ISO/IEC JTC1/SC29/WG1 Doc. N203.
- [9] J. Rissanen and G. G. Langdon, Jr., “Universal modeling and coding,” *IEEE Trans. Inform. Theory*, vol. IT-27, pp. 12–23, Jan. 1981.
- [10] J. Rissanen, “Generalized Kraft inequality and arithmetic coding,” *IBM J. Res. Develop.*, vol. 20, no. 3, pp. 198–203, May 1976.
- [11] M. J. Weinberger, J. Rissanen, and R. B. Arps, “Applications of universal context modeling to lossless compression of gray-scale images,” *IEEE Trans. Image Processing*, vol. 5, pp. 575–586, Apr. 1996.
- [12] M. J. Weinberger and G. Seroussi, “Sequential prediction and ranking in universal context modeling and data compression,” *IEEE Trans. Inform. Theory*, vol. 43, pp. 1697–1706, Sept. 1997. Preliminary version presented at 1994 IEEE Int. Symp. Inform. Theory, Trondheim, Norway, July 1994.
- [13] S. Todd, G. G. Langdon Jr., and J. Rissanen, “Parameter reduction and context selection for compression of the gray-scale images,” *IBM J. Res. Develop.*, vol. 29, pp. 188–193, Mar. 1985.
- [14] G. G. Langdon Jr., A. Gulati, and E. Seiler, “On the JPEG model for lossless image compression,” in *Proc. 1992 Data Compression Conf.*, Snowbird, UT, USA, Mar. 1992, pp. 172–180.
- [15] G. G. Langdon Jr. and M. Manohar, “Centering of context-dependent components of prediction error distributions,” *Proc. SPIE*, vol. 2028, pp. 26–31, July 1993.
- [16] G. G. Langdon Jr. and C. A. Haidinyak, “Experiments with lossless and virtually lossless image compression algorithms,” *Proc. SPIE*, vol. 2418, pp. 21–27, Feb. 1995.
- [17] X. Wu and N. D. Memon, “Context-based, adaptive, lossless image coding,” *IEEE Trans. Commun.*, vol. 45, pp. 437–444, Apr. 1997.
- [18] X. Wu, “Efficient lossless compression of continuous-tone images via context selection and quantization,” *IEEE Trans. Image Processing*, vol. 6, pp. 656–664, May 1997.
- [19] B. Meyer and P. Tischer, “TMW—A new method for lossless image compression,” in *Proc. 1997 Int. Picture Coding Symp.*, Berlin, Germany, Sept. 1997.
- [20] *Digital Compression and Coding of Continuous Tone Still Images—Requirements and Guidelines*, Sept. 1993. ISO/IEC 10918-1, ITU Recommend. T.81.
- [21] A. Netravali and J. O. Limb, “Picture coding: A review,” *Proc. IEEE*, vol. 68, pp. 366–406, 1980.
- [22] D. Huffman, “A method for the construction of minimum redundancy codes,” *Proc. IRE*, vol. 40, pp. 1098–1101, 1952.
- [23] M. Feder and N. Merhav, “Relations between entropy and error probability,” *IEEE Trans. Inform. Theory*, vol. 40, pp. 259–266, Jan. 1994.
- [24] P. G. Howard and J. S. Vitter, “Fast and efficient lossless image compression,” in *Proc. 1993 Data Compression Conf.*, Snowbird, UT, Mar. 1993, pp. 351–360.
- [25] X. Wu, W.-K. Choi, and N. D. Memon, “Lossless interframe image compression via context modeling,” in *Proc. 1998 Data Compression Conf.*, Snowbird, UT, Mar. 1998, pp. 378–387.
- [26] R. Barequet and M. Feder, “SICLIC: A simple inter-color lossless image coder,” in *Proc. 1999 Data Compression Conf.*, Snowbird, UT, Mar. 1999, pp. 501–510.
- [27] J. Rissanen, *Stochastic Complexity in Statistical Inquiry*, London, U.K.: World Scientific, 1989.
- [28] —, “Universal coding, information, prediction, and estimation,” *IEEE Trans. Inform. Theory*, vol. IT-30, pp. 629–636, July 1984.
- [29] N. Merhav, M. Feder, and M. Gutman, “Some properties of sequential predictors for binary Markov sources,” *IEEE Trans. Inform. Theory*, vol. 39, pp. 887–892, May 1993.
- [30] M. J. Weinberger, J. Rissanen, and M. Feder, “A universal finite memory source,” *IEEE Trans. Inform. Theory*, vol. 41, pp. 643–652, May 1995.
- [31] P. A. Maragos, R. W. Schafer, and R. M. Mersereau, “Two-dimensional linear predictive coding and its application to adaptive predictive coding of images,” *IEEE Trans. Acoust., Speech, Signal Processing*, vol. ASSP-32, pp. 1213–1229, Dec. 1984.
- [32] S. W. Golomb, “Run-length encodings,” *IEEE Trans. Inform. Theory*, vol. IT-12, pp. 399–401, July 1966.
- [33] N. Merhav, G. Seroussi, and M. J. Weinberger, “Coding of sources with two-sided geometric distributions and unknown parameters,” *IEEE Trans. Inform. Theory*, vol. 46, pp. 229–236, Jan. 2000.
- [34] —, “Modeling and low-complexity adaptive coding for image prediction residuals,” in *Proc. 1996 Int. Conf. Image Processing*, vol. 2, Lausanne, Switzerland, Sept. 1996, pp. 353–356.
- [35] —, “Optimal prefix codes for sources with two-sided geometric distributions,” *IEEE Trans. Inform. Theory*, vol. 46, pp. 121–135, Jan. 2000.
- [36] R. Ohnishi, Y. Ueno, and F. Ono, “The efficient coding scheme for binary sources,” *IECE Jpn.*, vol. 60-A, pp. 1114–1121, Dec. 1977. In Japanese.
- [37] S. A. Martucci, “Reversible compression of HDTV images using median adaptive prediction and arithmetic coding,” in *Proc. IEEE Int. Symp. Circuits Syst.*, 1990, pp. 1310–1313.
- [38] G. Seroussi and M. J. Weinberger, “On adaptive strategies for an extended family of Golomb-type codes,” in *Proc. 1997 Data Compression Conf.*, Snowbird, UT, Mar. 1997, pp. 131–140.
- [39] R. F. Rice, “Some Practical Universal Noiseless Coding Techniques—Parts I–III,” Jet Propulsion Lab., Pasadena, CA, Tech. Reps. JPL-79-22, JPL-83-17, and JPL-91-3, Mar. 1979, Mar. 1983, Nov. 1991.
- [40] “FlashPix format specification,” Digital Imaging Group, July 1997. Ver. 1.0.1.
- [41] D. E. Knuth, “Dynamic Huffman coding,” *J. Algorithms*, vol. 6, pp. 163–180, 1985.
- [42] R. Gallager and D. V. Voorhis, “Optimal source codes for geometrically distributed integer alphabets,” *IEEE Trans. Inform. Theory*, vol. IT-21, pp. 228–230, Mar. 1975.
- [43] J. Teuhola, “A compression method for clustered bit-vectors,” *Inform. Process. Lett.*, vol. 7, pp. 308–311, Oct. 1978.
- [44] G. G. Langdon Jr., “An adaptive run-length coding algorithm,” *IBM Tech. Disclosure Bull.*, vol. 26, pp. 3783–3785, Dec. 1983.
- [45] E. Ordentlich, M. J. Weinberger, and G. Seroussi, “A low complexity modeling approach for embedded coding of wavelet coefficients,” in *Proc. 1998 Data Compression Conf.*, Snowbird, UT, Mar. 1998, pp. 408–417.
- [46] S.-Y. Li, “Fast constant division routines,” *IEEE Trans. Comput.*, vol. C-34, pp. 866–869, Sept. 1985.
- [47] *LOCO-A: An Arithmetic Coding Extension of LOCO-I*, June 1996. ISO/IEC JTC1/SC29/WG1 Doc. N342.
- [48] *Activity Level Classification Model (ALCM)*, 1995. Proposal submitted in response to the Call for Contributions for ISO/IEC JTC 1.29.12.

- [49] *Evaluation of JPEG-DCT as a Near-Lossless Function*, June 1995. ISO/IEC JTC1/SC29/WG1 Doc. N207.
- [50] *JPEG 2000 VM 5.02*, Sept. 1999. ISO/IEC JTC1/SC29/WG1 Doc. N1422.
- [51] J. Ziv and A. Lempel, "A universal algorithm for sequential data compression," *IEEE Trans. Inform. Theory*, vol. IT-23, pp. 337–343, May 1977.
- [52] *Progressive Bi-Level Image Compression*, 1993. ISO/IEC 11544, CCITT T.82.
- [53] R. B. Arps and T. K. Truong, "Comparison of international standards for lossless still image compression," *Proc. IEEE*, vol. 82, pp. 889–899, June 1994.
- [54] A. Zaccarin and B. Liu, "A novel approach for coding color quantized images," *IEEE Trans. Image Processing*, vol. 2, pp. 442–453, Oct. 1993.
- [55] D. Clunie, "Lossless compression of grayscale medical images," *Proc. SPIE*, vol. 3980, Feb. 2000.



**Marcelo J. Weinberger** (M'90–SM'98) was born in Buenos Aires, Argentina, in 1959. He received the Electrical Engineer degree from the Universidad de la República, Montevideo, Uruguay, in 1983, and the M.Sc. and D.Sc. degrees in electrical engineering from Technion—Israel Institute of Technology, Haifa, in 1987 and 1991, respectively.

From 1985 to 1992, he was with the Department of Electrical Engineering, Technion, joining the faculty for the 1991–1992 academic year. During 1992–1993, he was a Visiting Scientist at IBM

Almaden Research Center, San Jose, CA. Since 1993, he has been with Hewlett-Packard Laboratories, Palo Alto, CA. His research interests are in information theory and statistical modeling, including source coding, data and image compression, and sequential decision problems.

Dr. Weinberger is an Associate Editor for Source Coding for the IEEE TRANSACTIONS ON INFORMATION THEORY.



**Gadiel Seroussi** (M'87–SM'91–F'98) was born in Montevideo, Uruguay, in 1955. He received the B.Sc. degree in electrical engineering, and the M.Sc. and D.Sc. degrees in computer science from Technion—Israel Institute of Technology, Haifa, in 1977, 1979, and 1981, respectively.

From 1981 to 1987, he was with the faculty of the Computer Science Department, Technion. During the 1982–1983 academic year, he was a Postdoctoral Fellow at the Mathematical Sciences Department, IBM T. J. Watson Research Center, Yorktown

Heights, NY. From 1986 to 1988, he was a Senior Research Scientist with Cyclotomics Inc., Berkeley, CA. Since 1988, he has been with Hewlett-Packard Laboratories, Palo Alto, CA, where he leads the Information Theory Research Group. His research interests include the mathematical foundations and practical applications of information theory, error correcting codes, data and image compression, and cryptography. He has published numerous journal and conference articles in these areas, and is a co-author of the recent book *Elliptic Curves in Cryptography*.



**Guillermo Sapiro** (M'93) was born in Montevideo, Uruguay, on April 3, 1966. He received the B.Sc. (summa cum laude), M.Sc., and Ph.D. degrees from the Department of Electrical Engineering, Technion—Israel Institute of Technology, Haifa, in 1989, 1991, and 1993, respectively.

After post-doctoral research at the Massachusetts Institute of Technology, Cambridge, he became Member of Technical Staff at Hewlett-Packard Laboratories, Palo Alto, CA. He is currently with the Department of Electrical and Computer Engineering,

University of Minnesota, Minneapolis. He works on differential geometry and geometric partial differential equations, both in theory and applications in computer vision and image analysis.

He recently co-edited a special issue of the IEEE TRANSACTIONS ON IMAGE PROCESSING and will be co-editing a special issue of the *Journal of Visual Communication and Image Representation*. He was awarded the Gutwirth Scholarship for Special Excellence in Graduate Studies in 1991, the Ollendorff Fellowship for Excellence in Vision and Image Understanding Work in 1992, the Rothschild Fellowship for Post-Doctoral Studies in 1993, the Office of Naval Research Young Investigator Award in 1998, the Presidential Early Career Awards for Scientist and Engineers (PECASE) in 1988, and the National Science Foundation Career Award in 1999.